Nuclear Materials and Energy 19 (2019) 372–377

Contents lists available at ScienceDirect

Nuclear Materials and Energy

journal homepage: www.elsevier.com/locate/nme

Conduction-based model of the Scrape-Off Layer power sharing between inner and outer divertor in diverted low-density tokamak plasmas

R. Maurizio*,[a], B.P. Duval[a], B. Labit[a], H. Reimerdes[a], C. Theiler[a], C.K. Tsui[a,b], J. Boedo[b], H. De Oliveira[a], O. Février[a], U. Sheikh[a], M. Spolaore[c], K. Verhaegh[d,a], N. Vianello[c], M. Wensing[a], TCV Team, and The EUROfusion MST1 Team[1,2]

[a] École Polytechnique Fédérale de Lausanne (EPFL), Swiss Plasma Center (SPC), Lausanne CH-1015, Switzerland
[b] University of California San Diego (UCSD), San Diego, CA, United States
[c] Consorzio RFX, Euratom-ENEA Association, Corso Stati Uniti 4, Padova IT-45127, Italy
[d] York Plasma Institute, University of York, York, United Kingdom

ARTICLE INFO

Keywords:
Heat exhaust
SOL transport
Long-legged Single Null Divertor
Snowflake Divertor
In-out power sharing
TCV

ABSTRACT

A simple analytic model for the repartition of the Scrape-Off Layer (SOL) exhaust power between the inner and outer divertors in a diverted low-density tokamak plasma is introduced. Electron heat conduction is assumed to dominate the heat transport, from the outboard mid-plane to the divertor targets, with no heat sinks or sources in the SOL. Both divertor channels are in the attached, high-recycling regime. The model is in reasonable qualitative agreement with recent TCV experimental data and EMC3-Eirene simulations. For the Single Null divertor, it reproduces the experimentally observed increase in the power ratio between the inner and outer divertor plates of TCV, P_{in}/P_{out}, with increasing the outer divertor leg length or the outer target flux expansion. For the Snowflake Minus configuration, it reproduces the observed variation of P_{in}/P_{out} with X-point separation, although only for the reversed magnetic field direction. Within the model limitations, it provides a basic understanding of the power sharing in alternative divertor geometries.

1. Introduction

Most existing tokamak devices operate with the conventional Single-Null (SN) magnetic configuration, in which exhaust heat and particles are deposited onto an inner and an outer divertor target. Extrapolations to bigger fusion experiments, such as ITER, indicate target unmitigated peak heat fluxes exceeding material limits, resulting into unacceptable damages [3]. Operating the ITER divertor in the partially detached regime [4] will greatly mitigate these heat fluxes, but it is not certain whether the reduction extrapolates to a fusion plant such as DEMO. Since it is usually observed that the inner target receives less power than the outer target and detaches at lower plasma densities, the outer target is much more a concern than the inner one [5,6]. Investigation of alternative magnetic configurations as a possible way to solve the power exhaust issue have, therefore, mainly focussed on the outer divertor.

Recent experiments on the TCV tokamak [1] have shown that the repartition of Scrape-Off Layer (SOL) exhaust power between the inner and outer divertor targets in an attached divertor regime depends on the magnetic divertor geometry. In the conventional Single-Null configuration, a longer poloidal length of the outer divertor leg or a larger flux expansion at the outer divertor target both result in more power to the inner target P_{in} and less to the outer target P_{out}, with fixed $P_{in} + P_{out}$ [7]. In the Snowflake Minus (SF-) configuration, a larger spatial distance between primary and secondary separatrix results in an increased P_{in} and a decreased P_{out}, again with fixed $P_{in} + P_{out}$ [8]. The TCV experiments suggest that an advanced magnetic configuration which is a solution for the outer divertor may actually worsen the conditions at the inner target.

With the aim of providing a possible, basic explanation of the experimentally observed effect of divertor geometry on divertor power sharing, this paper extends the analytic model proposed in [7] to divertor configurations with significant changes in the target radius and secondary x-points in the SOL, as for example in the SF- configuration. The model, presented in Section 2, is then compared to TCV measurements for the SN and SF- configurations in Section 3 and to fluid

* Corresponding author.
E-mail address: roberto.maurizio@epfl.ch (R. Maurizio).
[1] See the author list of Coda et al. [1].
[2] See the author list of Meyer et al. [2].

https://doi.org/10.1016/j.nme.2019.03.020
Received 13 August 2018; Received in revised form 18 March 2019; Accepted 22 March 2019
Available online 27 March 2019

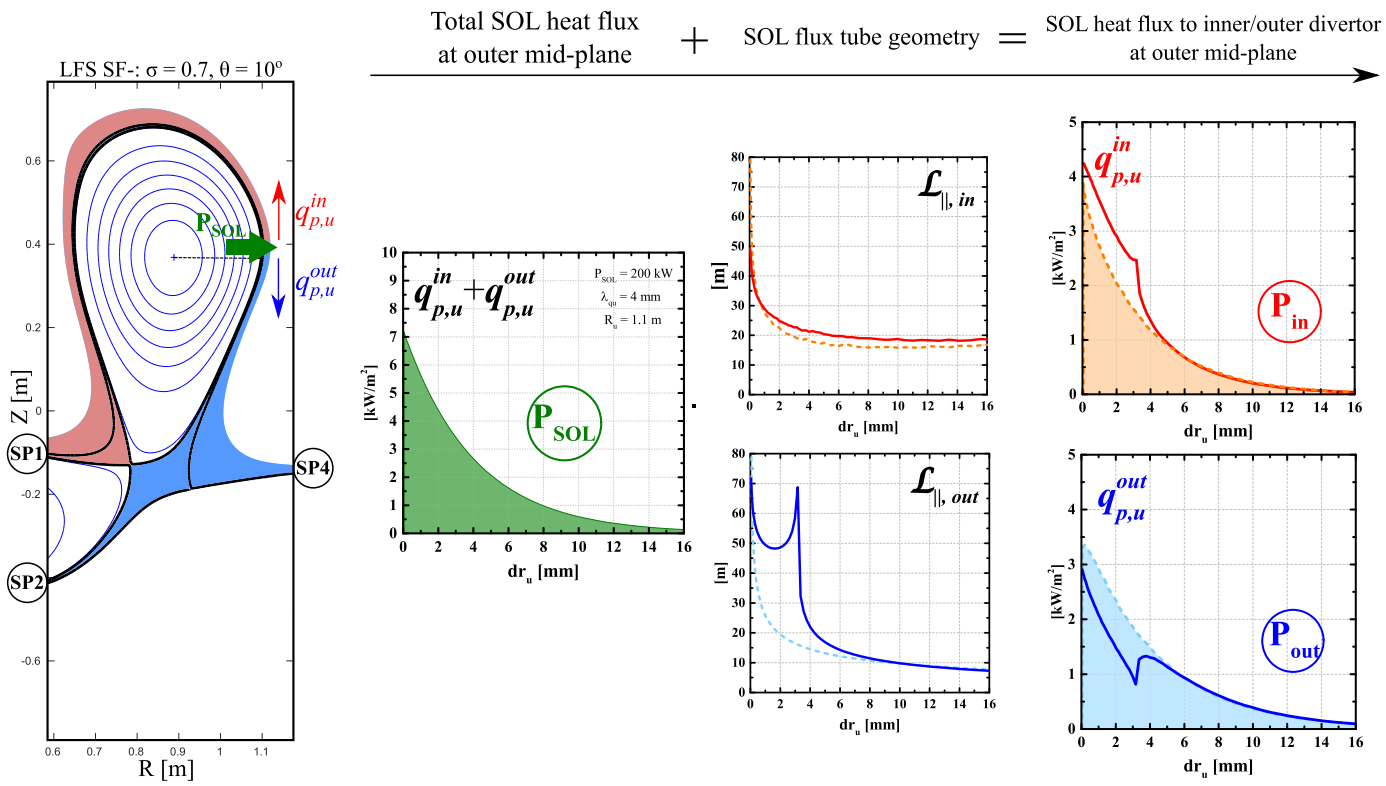

Fig. 1. Schematic of the model for the SOL power sharing between inner and outer divertors, illustrated, as an example, for a LFS Snowflake Minus divertor with $(\sigma, \theta) = (0.7, 10^{\circ})$ (continuous lines), and $(\sigma, \theta) = (0.1, 10^{\circ})$ (dashed lines). For a definition of (σ, θ), see Section 4. In the latter configuration, due to the very small x-point distance, the outer SOL (in blue) connects entirely to SP4. For each configuration, the upstream SOL poloidal heat flux profile (green) is repartitioned in two profiles, to the inner ($q^{\text{in}}_{p,u}$, red) and to the outer ($q^{\text{out}}_{p,u}$, blue) divertor, by considering the flux tubes' effective connection length for the inner, $\mathcal{L}_{\parallel,\text{in}}$, and outer, $\mathcal{L}_{\parallel,\text{out}}$, divertor. (For interpretation of the references to colour in this figure legend, the reader is referred to the web version of this article.)

simulations of the SF- configuration in Section 4. Conclusions are provided in Section 5.

2. Model of the SOL power sharing between divertors

The model proposed here combines the Onion-Skin Method procedure with the basic hypotheses of the Two-Point Model [10]. Electron heat conduction is assumed to dominate heat transport along magnetic field lines towards the divertor targets. Classical particle drifts in the SOL, which can explain the dependence of divertor power sharing on magnetic field direction [11–14], are here not considered.

The exhaust power P_{SOL} is taken to enter the SOL at the outer mid-plane ("upstream"), where it separates into one flow towards the inner divertor (P_{in}) and another to the outer divertor (P_{out}), see Fig. 1. The model assumes that both divertor legs are attached and in the high-recycling regime, and the SOL harbours no volume particle sinks or sources.

Any location in the SOL at the outer mid-plane is simultaneously connected through two separate flux tubes to both the inner and outer divertors. For a given upstream location, the parallel heat flux conducted towards each target [10]

$$q_{\parallel}(s_{\parallel}) = -\kappa_0^e \, T(s_{\parallel})^{5/2} \frac{\mathrm{d}T}{\mathrm{d}s_{\parallel}}$$

is readily integrated along a flux tube, from the upstream location ($s_{\parallel} = 0$, major radius R_u) to the divertor target ($s_{\parallel} = L_{\parallel}$, major radius R_t). With the assumption of an upstream temperature T_u being much higher than at the target and using the invariance of $q_{\parallel}(s_{\parallel}) \cdot R(s_{\parallel})$ along the flux tube, the parallel heat flux entering the flux tube at the upstream location is

$$q_{\parallel,u} = \frac{2\,\kappa_0^e\, T_u^{7/2}}{7\,\mathcal{L}_{\parallel}} \tag{1}$$

where

$$\mathcal{L}_{\parallel} = \int_0^{L_{\parallel}} \mathrm{d}s_{\parallel} \, \frac{R_u}{R(s_{\parallel})} \tag{2}$$

is the parallel connection length of the flux tube, $L_{\parallel}$, weighted by the inverse major radius. In the following, $\mathcal{L}_{\parallel}$ is referred to as the effective parallel connection length. Note that if one neglects the variation of R along the flux tube, $\mathcal{L}_{\parallel} = L_{\parallel}$.

Since the upstream temperatures deduced for the inner and outer divertor with Eq. (1) must be the same, the sharing of power between the inner and outer divertor, for the selected flux tube, is

$$q^{\text{in}}_{\parallel,u}/q^{\text{out}}_{\parallel,u} = \mathcal{L}_{\parallel,\text{out}}/\mathcal{L}_{\parallel,\text{in}} \tag{3}$$

Thus the flux tube geometry, alone, determines the sharing of heat flux between the divertors. Long and narrow flux tubes (i.e. with small major radius R, since the cross-sectional area scales as $\propto R$) have a greater $\mathcal{L}_{\parallel}$ than short and broad flux tubes and therefore conduct less heat to the plates for a given upstream-to-target temperature drop. Eq. (3) can be formulated in terms of the component of the heat flux in the poloidal plane:

$$q^{\text{in}}_{p,u}/q^{\text{out}}_{p,u} = \mathcal{L}_{\parallel,\text{out}}/\mathcal{L}_{\parallel,\text{in}} \tag{4}$$

since $q_{p,u} = (B_{p,u}/B_{\text{tot},u})\, q_{\parallel,u}$, with $B_{p,u}$ and $B_{\text{tot},u}$ the upstream poloidal and total magnetic fields.

The methodology to compute the global power sharing for a magnetic geometry is discussed in the following. To obtain an estimate of the power sharing, the r.h.s. of Eq. (4) must be weighted across the SOL. It is, therefore, assumed that the SOL heat flux perpendicular to flux

surfaces can be described by an exponential with a characteristic fall-off length $\lambda_{q,u}$. With no heat sources in the SOL, the sum of $q^{in}_{p,u}$ and $q^{out}_{p,u}$ is an exponential with the same fall-off length

$$\left(q^{in}_{p,u} + q^{out}_{p,u}\right)(dr_u) = \frac{P_{SOL}}{2\pi R_u \lambda_{q,u}} e^{-dr_u/\lambda_{q,u}} \quad (5)$$

with dr_u the upstream distance from the separatrix and R_u the major radius at the outboard mid-plane. Then, $\mathcal{L}_{\parallel,in}$ and $\mathcal{L}_{\parallel,out}$ are calculated for each SOL magnetic surface with relation (2). For each upstream location, using Eqs. (4) and (5), the poloidal heat flux directed towards the inner divertor, $q^{in}_{p,u}$, and that directed towards the outer divertor, $q^{out}_{p,u}$, are computed, see Fig. 1. Finally, integration of these profiles over the entire SOL yields the net power entering the inner, P_{in}, and outer, P_{out}, divertor.

Note that assuming, alternatively, that the upstream SOL temperature profile is an exponential leads to very similar predictions and in particular no changes of the trends.

3. Comparison with TCV measurements

In this section, the power sharing between inner and outer divertor measured on TCV for several magnetic configurations, both conventional and advanced, is compared with the predictions from the proposed model. The experiments were carried out with L-mode deuterium plasmas, with a line-averaged density that corresponds to of the Greenwald density. The divertors are attached, in the high-recycling regime. The power deposited at the divertor targets is estimated from Infrared Thermography measurements [7].

3.1. Single Null configuration

In the conventional SN configuration, the exhaust power is deposited at the inner (ISP) and at the outer (OSP) strike point, Fig. 2(a), so that $P_{in}/P_{out} = P_{ISP}/P_{OSP}$.

The power sharing model can qualitatively reproduce the experimentally observed increase of P_{in}/P_{out} when increasing the outer divertor leg poloidal length L_{div}, Fig. 2(d), or the outer divertor target flux expansion f_x, Fig. 3(d). The L_{div} was varied in discharges with a plasma current of 210 kA and the magnetic field in the forward direction, i.e. with the ion ∇B drift directed towards the X-point. Increasing L_{div} from 20 to 65 cm results into an increase of P_{in}/P_{out} from 0.36 to 0.75 with the model predicting an increase from 0.68 to 1.26. The f_x was varied in discharges with a plasma current of 340 kA and the magnetic field in the reversed direction, i.e. with the ion ∇B drift directed away from the X-point. Increasing f_x from 2 to 9 results into an increase of P_{in}/P_{out} from 0.60 to 0.95 with the model predicting an increase from 0.83 to 1.36. With the offset between model estimates and data being smaller in the reversed field direction, it is thought to be a combined effect of in-out asymmetric volumetric radiative losses and classical $\vec{E} \times \vec{B}$ drifts, both not included in the model. Note that the model predictions are fairly insensitive to the assumed value of $\lambda_{q,u}$, with a factor two change in $\lambda_{q,u}$ resulting in $< 10\%$ change in P_{in}/P_{out}.

According to the model, this power sharing variation is caused by the increased parallel connection length to the outer target, Figs. 2(b) and 3(b). These TCV measurements show that, in attached conditions, an increased parallel connection length to the outer divertor reduces the peak heat fluxes at the outer target but increases those at the inner target.

3.2. LFS Snowflake Minus configuration

In the SF- configuration, a secondary null is placed in the common flux region of the primary null and is associated to a secondary separatrix. This splits the SOL into two manifolds, such that three out of four strike points (named SP1 through SP4) are connected to the upstream SOL, see Fig. 4(a) and (c). For the LFS (Low-Field Side) SF- variant, Fig. 4(a), $P_{in}/P_{out} = P_{SP1}/(P_{SP2} + P_{SP4})$. For the HFS (High-Field Side) SF- variant, Fig. 4(d), $P_{in}/P_{out} = (P_{SP1} + P_{SP3})/P_{SP4}$. In a study on TCV [8], the distance between primary and secondary separatrix evaluated at the outer mid-plane, dr_{x2}, was gradually increased to study the effect of divertor geometry changes on power repartition between targets. The experiments were carried out at 240 kA and both magnetic field directions. The study showed that the location of the secondary x-point has a great impact on the SOL connection length profiles as well as on the target radius.

For the reversed field direction (RF, ion ∇B drift upwards), the power sharing model qualitatively reproduces the observed variation of P_{in}/P_{out} when increasing dr_{x2}. In the LFS SF-, Fig. 4(c), when changing dr_{x2} from 0 to 7 mm, the measured P_{in}/P_{out} increases from 0.7 to 1.4 and the modelled from 1.4 to 1.6. In the HFS SF-, Fig. 4f), when changing dr_{x2} from 0 to 5 mm, both measured and modelled P_{in}/P_{out} decrease from 0.7 to 0.55.

For the forward field direction (FF, ion ∇B drift downwards), however, the power sharing model cannot explain the variation of P_{in}/P_{out}. In the LFS SF-, Fig. 4(b), when changing dr_{x2} from 0 to 12 mm, the measured P_{in}/P_{out} increases from 0.3 to 0.9 while the modelled decreases from 2.1 to 1.5. In the HFS SF-, Fig. 4(e), when changing dr_{x2} from 0 to 4 mm, the measured P_{in}/P_{out} increases from 0.25 to 0.5 while the modelled decreases from 9 to 0.6. Note that for both field directions, and similarly to the SN case, the model predictions are fairly insensitive to the assumed value of $\lambda_{q,u}$, as shown in Fig. 4.

The disagreement between model and data for the forward field

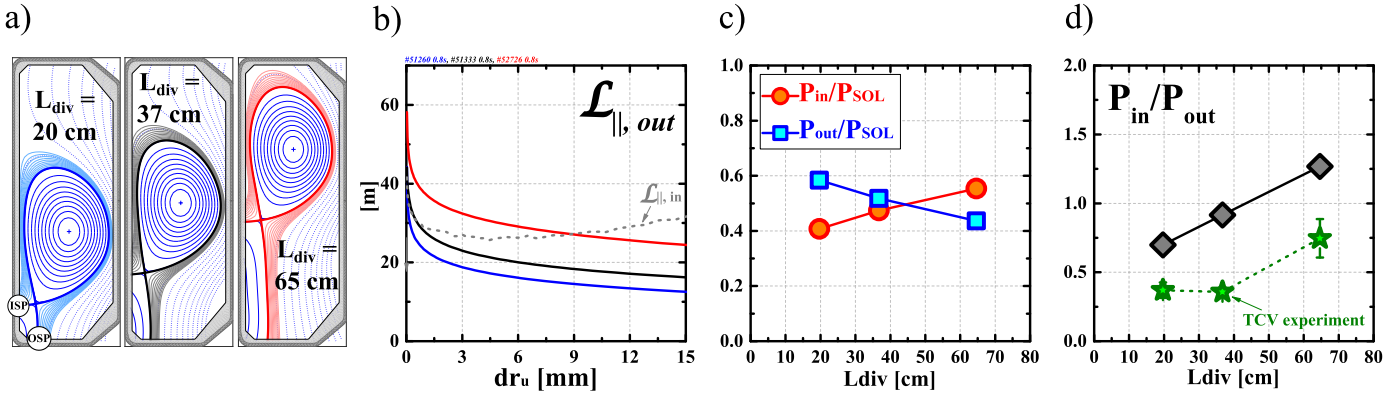

Fig. 2. Scan of the outer divertor leg length L_{div}, for forward field direction, outer target $f_x = 3.5$, plasma current $I_P = 210$ kA and SOL width $\lambda_{q,u} = 5$ mm (typical value for this I_P).(a) TCV magnetic equilibria. (b) Profiles of the effective parallel connection length in the SOL. (c) Fraction of exhaust power to each divertor, from the model, as a function of L_{div}. (d) Power sharing ratio, experimental (green stars) and from the model (grey diamonds), as a function of L_{div}. (For interpretation of the references to colour in this figure legend, the reader is referred to the web version of this article.)

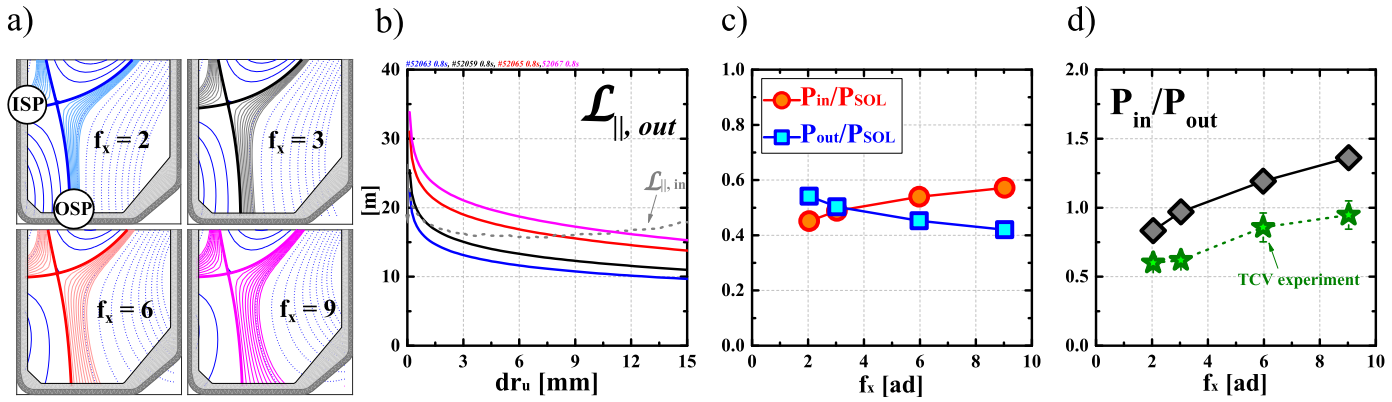

Fig. 3. Scan of the outer target flux expansion f_x, for reversed field direction, $L_{div} = 38.5$ cm, plasma current $I_P = 340$ kA and SOL width $\lambda_{q,u} = 3$ mm (typical value for this I_P).(a) TCV magnetic equilibria. (b) Profiles of the effective parallel connection length in the SOL. (c) Fraction of exhaust power to each divertor, from the model, as a function of f_x. (d) Power sharing ratio, experimental (green stars) and from the model (grey diamonds), as a function of f_x. (For interpretation of the references to colour in this figure legend, the reader is referred to the web version of this article.)

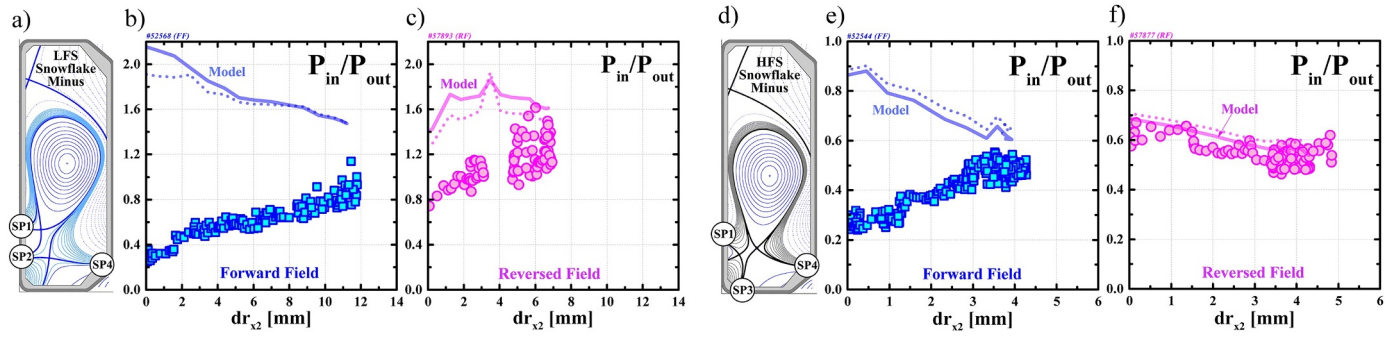

Fig. 4. Measured inner/outer divertor power ratio, for the LFS SF- (a)–(c) and HFS SF- (d)–(f) configurations, in forward field (blue squares) and reversed field (purple circles) conditions, compared to the predictions from the model for $\lambda_{q,u} = 4$ mm (continuous line) and $\lambda_{q,u} = 6$ mm (dashed line). (For interpretation of the references to colour in this figure legend, the reader is referred to the web version of this article.)

direction clearly indicates that the analytical model misses physics that in the SF- divertor dominate over heat conduction. As for the Single Null configurations, discussed in Section 3.1, it is hypothesised that this could be the combined effect of asymmetric divertor radiation and poloidal $\vec{E} \times \vec{B}$ classical drifts [10,15], which may have an even larger effect in the SF configuration [16].

4. Comparison to fluid simulations of the LFS SF-

This section considers some TCV-sized LFS SF- configurations and compares the power sharing between inner and outer divertor computed by EMC3-Eirene fluid calculations [9], assuming constant cross-field transport coefficients, to that predicted by the model. To investigate the effect of the x-point position on power repartition between strike points, each geometrical parameter of the SF configuration, σ and θ, was varied while keeping the other constant. σ is the spatial distance, in the poloidal plane, between the two x-points, normalized on the plasma minor radius, while θ is the angle between a line connecting the x-points and a line perpendicular to the segment connecting the magnetic axis and the primary x-point [17]. Note that, for the fluid simulations here discussed, the fraction of input power deposited to the targets is $\approx 60\%$, independently of σ or θ (variations $< 5\%$).

The power sharing model reproduces the increase of P_{in} and the decrease of P_{out} showed by the fluid calculations when increasing σ, Fig. 5(c), as well as the resultant increase of P_{in}/P_{out}, Fig. 5(d). When changing σ from 0.1 to 0.9, the fluid calculation P_{in}/P_{out} increases from 0.73 to 1.32 and the modelled from 0.82 to 1.57. A trend agreement between model and simulations is found also for the scan of θ, Fig. 6(c) and (d). When changing θ from 10° to 35°, the fluid calculation P_{in}/P_{out} weakly increases from 1.17 to 1.37 and the modelled from 1.71 to 2. In all cases, the deposited power given by fluid calculations is lower than that predicted by the power sharing model. This is most likely because charge exchange and elastic collisions with the neutral gas, as well as radiation, are considered in the fluid calculations but are not included in the model.

It is interesting to further investigate how variations of σ and θ in a LFS SF- change the flux tube geometry and thus the power sharing.

When σ is increased at fixed θ, some flux tubes formerly connected to SP4 connect to SP2, Fig. 5(a), and their connection lengths increase, because of the low poloidal field in the intra-null region, and their major radius, on average, decrease. This enhances $\mathcal{L}_{||,out}$, Fig. 5(b), which in turn limits the heat that can be conducted to SP2, Eq. (3). The flux tubes connecting the same upstream location to SP1 will, in addition, exhaust this difference, Fig. 5(c).

When θ is increased at fixed $\sigma = 1$, some flux tubes formerly intercepting SP2 connect to SP4, Fig. 6(a). Their $\mathcal{L}_{||,out}$ reduces ($L_{||}$ decreases and the major radius, on average, increases), so conduct more heat to the target. In contrast, for the flux tubes connected to SP2, $\mathcal{L}_{||,out}$ increases, since the secondary null approaches the divertor leg, Fig. 6(a), reducing the poloidal field and thus augmenting the $L_{||}$, Fig. 6(b). This limits the power that can be conducted to SP2. These two effects approximately balance, so P_{out} does not change with increasing θ, Fig. 6(c).

Evaluating the power sharing model, for the LFS SF- geometries of Fig. 5(a), for a range of $\lambda_{q,u}$ shows that the ratio P_{in}/P_{out} scales as $\propto dr_{x2}/\lambda_{q,u}$ and quickly saturates for $dr_{x2}/\lambda_{q,u} > 2$. This is explained by the fraction of the SOL heat flux profile, enclosed between primary and secondary separatricies, which is proportional to $dr_{x2}/\lambda_{q,u}$.

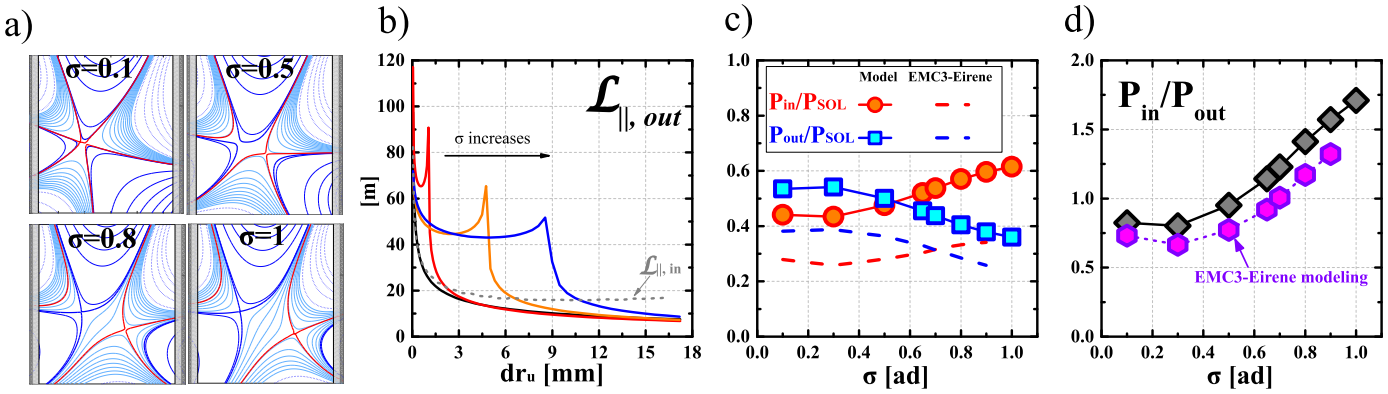

Fig. 5. In a LFS SF- configuration, scan of the x-point distance σ at fixed $\theta = 10°$ and $\lambda_{q,u} = 4$ mm. (a) SPIDER magnetic equilibria. (b) Profiles of the effective parallel connection length in the SOL. (c) Fraction of exhaust power to each divertor, from the model, as a function of σ. (d) Power sharing ratio, from the model (grey diamonds) and from fluid calculations [9] (purple hexagons), as a function of σ. (For interpretation of the references to colour in this figure legend, the reader is referred to the web version of this article.)

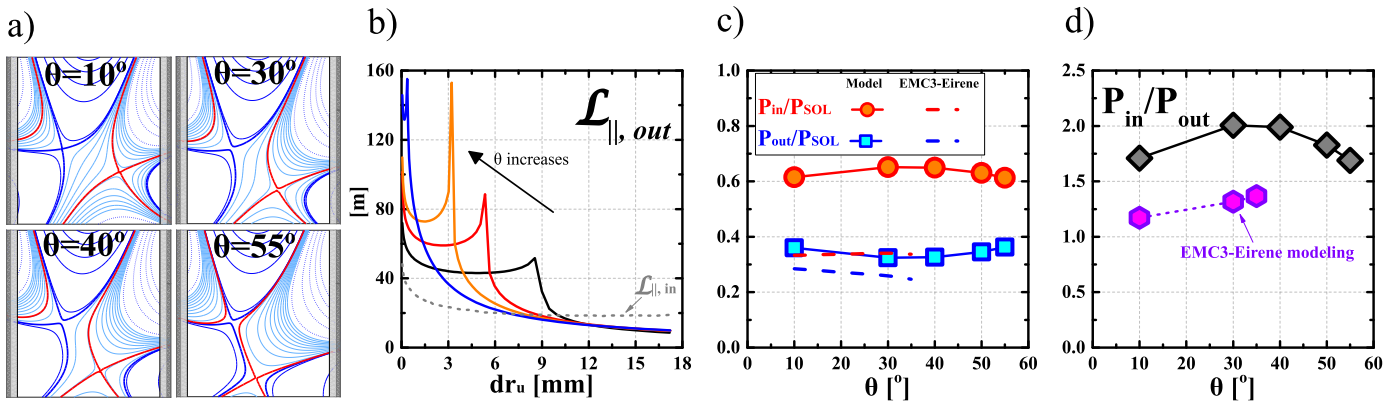

Fig. 6. In a LFS SF- configuration, scan of θ at fixed $\sigma = 1$ and $\lambda_{q,u} = 4$ mm. (a) SPIDER magnetic equilibria. (b) Profiles of the effective parallel connection length in the SOL. (c) Fraction of exhaust power to each divertor, from the model, as a function of θ. (d) Power sharing ratio, from the model (grey diamonds) and from fluid calculations [9] (purple hexagons), as a function of θ. Note that the fluid calculations use equilibria with slightly increasing $\sigma \approx (0.8; 0.92; 1.15)$. (For interpretation of the references to colour in this figure legend, the reader is referred to the web version of this article.)

5. Conclusions and outlook

This paper presents and discusses a simple analytic model of the SOL power sharing between inner and outer divertors in a low-density tokamak diverted plasma, where both divertors are in the high-recycling regime. The heat flux is taken to leave the confined volume and enter the SOL at the out-board mid-plane, and is then transported parallel to magnetic field lines towards the divertor targets by electron heat conduction, without any intervening heat sinks or sources and no contribution from classical particle drifts.

The prediction for the in-out power sharing for a series of magnetic configurations is compared to recent TCV experimental data and previously published EMC3-Eirene simulations.

For the conventional Single Null (SN) divertor, the model can reproduce the experimentally observed increase in the power ratio between the inner/outer divertor plates, P_{in}/P_{out}, when increasing either the poloidal length of the outer divertor leg or the outer target flux expansion. These TCV measurements show that, in attached conditions, an increased parallel connection length to the outer divertor reduces the peak heat fluxes at the outer target but increases those at the inner target. This reveals that a power exhaust solution at the outer divertor achieved via modifications of the magnetic configuration may come at the expense of the inner divertor.

For the Snowflake Minus (SF-) divertor, the model can reproduce the observed variations of P_{in}/P_{out} with the separatrix distance dr_{x2}, albeit solely for the reversed magnetic field direction. The disagreement in the forward field direction clearly indicates that the analytical model misses physics that in the SF- dominates over heat conduction. It is hypothesised that this could be a combined effect of asymmetric divertor radiation and poloidal $\vec{E} \times \vec{B}$ classical drifts in the SOL. The model also reproduces the increase of P_{in}/P_{out} with increasing σ and its insensitivity to θ that were calculated in EMC3-Eirene simulations of the LFS SF- divertor.

Conflict of interests

The authors declare that they have no known competing financial interests or personal relationships that could have appeared to influence the work reported in this paper.

Acknowledgements

The authors thank Dr. T. Lunt and the TCV boundary physics group for helpful and constructive discussions. This work has been carried out within the framework of the EUROfusion Consortium and has received funding from the Euratom research and training programme 2014-2018 under grant agreement no. 633053. The views and opinions expressed herein do not necessarily reflect those of the European Commission. This work was supported in part by the Swiss National Science Foundation.

Supplementary material

Supplementary material associated with this article can be found, in the online version, at 10.1016/j.nme.2019.03.020.

References

[1] S. Coda, et al., Overview of the TCV tokamak program: scientific progress and facility upgrades, Nucl. Fusion 57 (10) (2017) 102011, https://doi.org/10.1088/1741-4326/aa6412.

[2] H. Meyer, et al., Overview of progress in European medium sized tokamaks towards an integrated plasma-edge / wall solution, Nucl. Fusion 57 (10) (2017) 102014, https://doi.org/10.1088/1741-4326/aa6084.

[3] T. Eich, et al., Scaling of the tokamak near the scrape-off layer H-mode power width and implications for ITER, Nucl. Fusion 53 (9) (2013) 093031, https://doi.org/10.1088/0029-5515/53/9/093031.

[4] A. Kallenbach, et al., Optimized tokamak power exhaust with double radiative feedback in ASDEX upgrade, Nucl. Fusion 52 (12) (2012) 122003, https://doi.org/10.1088/0029-5515/52/12/122003.

[5] C.S. Pitcher, P.C. Stangeby, Experimental divertor physics, Plasma Phys. Control. Fusion 39 (6) (1997) 779–930, https://doi.org/10.1088/0741-3335/39/6/001.

[6] A. Herrmann, et al., Overview on stationary and transient divertor heat loads, Plasma Phys. Control. Fusion 44 (2002) 897–917, https://doi.org/10.1088/0741-3335/44/6/319.

[7] R. Maurizio, et al., Divertor power load studies for attached L-mode single-null plasmas in TCV, Nucl. Fusion 58 (1) (2018) 016052, https://doi.org/10.1088/1741-4326/aa986b.

[8] R. Maurizio, et al., The effect of the secondary x-point on the Scrape-Off Layer transport in the TCV Snowflake Minus divertor, Nucl. Fusion 59 (1) (2019) 016014, https://doi.org/10.1088/1741-4326/aaee1b.

[9] T. Lunt, et al., Numerical study of potential heat flux mitigation effects in the TCV snowflake divertor, Plasma Phys. Control. Fusion 58 (4) (2016) 045027, https://doi.org/10.1088/0741-3335/58/4/045027.

[10] P. Stangeby, The Plasma Boundary of Magnetic Fusion Devices, Institute of Physics Publishing Bristol and Philadelphia, 2000.

[11] P. Stangeby, et al., Simple models for the radial and poloidal $\vec{E} \times \vec{B}$ drifts in the scrape-off layer of a divertor tokamak: effects on in/out asymmetries, Nucl. Fusion 36 (7) (1996) 839–852, https://doi.org/10.1088/0029-5515/36/7/I02.

[12] A. Loarte, et al., Multi-machine scaling of the divertor peak heat flux and width for L-mode and H-mode discharges, J. Nucl. Mater. 266 (1999) 587–592, https://doi.org/10.1016/S0022-3115(98)00590-X.

[13] A. Chankin, et al., Toroidal field reversal effects on divertor asymmetries in JET, Plasma Phys. Control. Fusion 38 (1996) 1579–1592, https://doi.org/10.1088/0741-3335/38/9/004.

[14] R. Pitts, et al., Edge and divertor physics with reversed toroidal field in JET, J. Nucl. Mater. 337–339 (2005) 146–153, https://doi.org/10.1016/j.jnucmat.2004.10.111.

[15] N. Christen, et al., Exploring drift effects in TCV Single-Null plasmas with the UEDGE code, Plasma Phys. Control. Fusion 59 (10) (2017) 105004, https://doi.org/10.1088/1361-6587/aa7c8e.

[16] G. Canal, et al., Enhanced $\vec{E} \times \vec{B}$ drift effects in the TCV snowflake divertor, Nucl. Fusion 55 (12) (2015) 123023, https://doi.org/10.1088/0029-5515/55/12/123023.

[17] D. Ryutov, et al., The snowflake divertor, Phys. Plasmas 22 (11) (2015) 110911, https://doi.org/10.1063/1.4935115.